Community Metabolic Modeling Unlocks the Potential of Thermophilic Synthetic Communities for Enhanced Butyric Acid Production

Gustavo Lastiri-Pancardo[1], Lizzete Moreno[2], Neal N. Hengge[3], Manish Kumar[1], Jeffrey G. Linger[2], Violetta Sanchez i Nogue[2], Michael T. Guarneri[3], Karsten Zengler[1,3,4,5,6*]

[1]Department of Pediatrics, University of California, San Diego, 9500 Gilman Drive, La Jolla, CA 92093-0760, USA
[2]Renewable Resources and Enabling Sciences Center, National Renewable Energy Laboratory, 15013 Denver West Pkwy, Golden, CO 80401, USA
[3]Biosciences Center, National Renewable Energy Laboratory, 15013 Denver West Pkwy, Golden, CO 80401, USA
[4]Department of Bioengineering, University of California, San Diego, La Jolla CA 92093-0412, USA
[5]Center for Microbiome Innovation, University of California, San Diego, La Jolla, CA 92093-0403, USA
[6]Program in Materials Science and Engineering, University of California, San Diego, La Jolla, CA 92093-0418, USA

*Corresponding author: Karsten Zengler (kzengler@ucsd.edu)

Abstract

The intricate network of interspecies interactions within microbial communities drives their functional organization, enabling them to perform complex tasks like breaking down resistant lignocellulosic materials into volatile fatty acids (VFAs). Butyric acid (BA), a VFA, is gaining attention for its applications in sustainable aviation fuel, polymers, fibers, and cosmetics. However, the need for costly enzymatic pre-treatment of lignocellulosic substrates limits the economic viability of a biosustainable production process. This study experimentally demonstrated the effectiveness of a mutualistic co-culture of thermophilic bacteria *Clostridium thermocellum* and *Clostridium thermobutyricum* in converting lignocellulose to BA without enzymatic pre-treatment. Despite >100% enhancement in substrate utilization compared to mono-culture, significant carbohydrates and fermentation byproducts remained unused. Using high-quality, manually curated genome-scale metabolic models (GEMs), the metabolic interactions within the co-culture were characterized, and bottlenecks that contribute to incomplete substrate utilization were identified. This research highlights the potential of co-cultures and synthetic communities in sustainable bioproduction.

Introduction

Bacterial communities are ubiquitous in nature, forming elaborate relationships and interactions that enable them to perform tasks unattainable by single members (Zuñiga *et al*., 2020, Coker *et al*., 2022). One such task involves the breakdown of plant-derived material into volatile fatty acids (VFAs), including acetic, lactic, and butyric acid (BA) (Agnihotri *et al*., 2022). BA is a particularly valuable fermentation product because of its widespread use as a versatile platform chemical in the food and pharmaceutical industry. BA holds immense potential as a precursor for various applications, such as fiber production, polymer synthesis, as well as production of cosmetics, and aviation fuels (Linger *et al*., 2020; Salvachúa *et al*., 2021). Currently, BA is primarily synthesized from petroleum, which is not only costly but also not sustainable.

Numerous bioprocesses have been suggested for utilizing renewable substrates from lignocellulosic sources to produce VFA, including BA (Linger *et al*., 2020; Salvachúa *et al*., 2021). However, these processes commonly depend on single microorganisms and necessitate biomass preprocessing steps using enzymatic, chemical, and/or mechanical deconstruction strategies, which are often costly and have diminished yields (Chen *et al*., 2014). To tackle this challenge, a novel approach for BA bioproduction has been proposed, utilizing a synthetic thermophilic bacterial co-culture. This approach involves the close interaction of the two thermophilic bacteria *Clostridium thermocellum* DSM1313 (CTC) and *Clostridium thermobutyricum* DSM4928 (CTB). CTC has gained attention for its remarkable proficiency in effectively breaking down insoluble and oligomeric lignocellulosic substrates, owing to a highly specialized multi-enzyme apparatus known as the cellulosome (Lamed *et al*., 1983; Hirano *et al*., 2016). This intricate structure found in several anaerobic bacteria such as *Bacteroides*, *Clostridium*, and *Ruminococcus* (Doi *et al*., 2003) comprises primary and secondary scaffolding proteins, serving as anchoring point for a wide variety of hydrolytic enzymes, including cellulases, hemicellulases, and pectinases. On the other hand, CTB demonstrates high efficiency in converting a wide range of monomeric carbohydrates into BA (Wiegel *et al*., 1989). When combined as co-culture, CTC and CTB can effectively convert lignocellulosic substrates into BA in a single-step process, bypassing the costly and inefficient preprocessing step (Chi *et al*., 2018). Furthermore, such consolidated bioprocessing for production of VFA at elevated temperatures has been demonstrated to offer advantages and cost-effectiveness (Hao & Wang, 2015). Thus, this thermophilic and effective co-culture offers a promising approach for the sustainable production of BA as an industrially relevant chemical.

Constraint-based metabolic modeling is a powerful tool in systems biology that offers a comprehensive understanding of the metabolism of individual microorganisms, i.e. metabolic models or M-models, as well as microbial communities, i.e. community metabolic models, CM-models. These genome-scale metabolic models (GEMs) are reconstructions of the entire metabolic network of a cell, incorporating all biochemical and multi-omics information available for a specific microbe and allowing for a detailed mechanistic

understanding of metabolic processes (Bordbar *et al*., 2014; Kumar *et al*., 2019). GEMs can accurately predict a multitude of functional states of a cell, providing valuable insights into the metabolic and production capabilities of microorganisms. Expanding this framework to communities has demonstrated unprecedented capabilities in unraveling the complex and dynamic interactions of multiple microbes (Zengler *et al*., 2018; Zuñiga *et al*., 2019; Zaramela *et al*., 2021).

Here, a CTC-CTB corn stover to BA system was established and experimentally characterized, including the substrate utilization and product formation capacity of mono- and co-cultures. Comprehensive GEMs for CTC (iGL735) and CTB (iGL834) were subsequently constructed. Additionally, these individual models were integrated into a highly curated CM-model (iGL^{2}1559). The modeling framework was employed to unveil interactions and provide a mechanistic insight into BA production from lignocellulosic substrates, paving the way for the development of a thermophilic and sustainable bioprocess based on a synthetic CTC-CTB co-culture.

Results

Reconstruction and refinement of the individual M-models for two thermophilic anaerobes

An initial version of a GEM of CTC was constructed using as a foundation the most recent metabolic reconstruction of this organism (*i*CBI655, Garcia *et al.*, 2020) and its genome annotation. Additionally, the first reported GEM for *C. thermobutyricum* (CTB) was constructed, leveraging the annotated genome information alongside highly curated M-models from other closely related species, including the previously developed CTC model, and models for *Clostridium ljungdahlii* (*i*HN637, Nagarahan *et al*., 2013), *Bacillus subtillis* (*i*YO844, Oh *et al*., 2007; *i*JT964-ME, Tibocha-Bonilla *et al*., 2022), and *Escherichia coli* (*i*EC1515, Monk *et al*., 2017), as well as protein sequence homology (Fig. 1A, Top).

To ensure the fidelity and robustness of our reconstructions, both M-models underwent an iterative process of manual curation and refinement. This curation led to the introduction of various modifications, spanning aspects such as mass and energy equilibrium adjustments, rectifying cofactor discrepancies, standardizing biomass metabolites among models, updating and repairing gene-reaction associations, broadening permissible metabolite exchanges, resolving infeasible flux cycles, and introducing or removing various metabolic reactions (See Methods) (Fig. 1A, Bottom).

For both organisms, the metabolic network was partitioned into two distinct compartments, the cytoplasm and the extracellular space. Additionally, a specialized compartment representing the cellulosome was defined for CTC. This unique compartment serves as a model of the fundamental enzymatic activities crucial for breaking down cellulose, hemicellulose, and other intricate polysaccharides. While the structure outlined in the M-model offers a generalized portrayal of CTC's mechanisms for degrading complex carbohydrates, it is important to acknowledge that due to lack of information, the cellulosome reconstruction might not fully capture the complete array of enzymes and specific processes employed in nature by this microorganism (Hirano *et al*., 2016).

The completed M-model for CTC, designated as *i*GL735, comprises 735 genes, 733 metabolites, and 780 reactions, covering 26.3% of the genome. The final M-model for CTB (*i*GL834) is composed of 834 genes, 790 metabolites, and 876 reactions, offering 27.2% of genomic coverage (Fig. 1B). A comparison between the generated GEMs and the various templates employed for their construction is presented in Table 1.

Building and evaluating a two-member CM-model

Subsequently, the individual M-models were merged to create a CM-model. These models offer a mathematical representation of the genomic and metabolic attributes of the microorganisms within a community, serving as essential instruments for investigating the metabolic interplay and synergies that emerge in shared environments. By amalgamating the separately constructed M-models of CTC and CTB, a two-member CM-model was

formulated. The model operates on the principle of a compartmentalized community, envisioning a scenario where various members reside within a common compartment and engage in the use and exchange of a shared metabolites pool (SMP) (Nagarajan *et al.,* 2013; Klitgord & Segrè, 2010). Within this framework, every nutrient and by-product generated by any individual member becomes accessible for consumption by all other participants in the community. This setup helps to model dynamic ecosystems where metabolic interactions occur seamlessly. At its core, the CM-model focuses on a linear objective, which involves the summation of biomass fluxes attributed to each organism within the community. This linear objective can be tuned to represent the different proportions in which each member is present and serves as a quantitative measure of the collective growth and productivity of the entire community, encapsulating the cumulative contributions of individual members (Fig. 1C).

Considering the metabolic exchange capacities of each member within the community, the SMP underwent meticulous manual curation. The resulting CM-model, designated as *i*GL^{2}1559, accounts for two organisms, totaling 1,559 genes and engaging in 1,777 reactions involving 1,679 metabolites, 37 of which are shared through the SMP (Fig. 1D). Each individual anaerobe possesses distinct metabolic pathways and functionalities inherent to its genetic and biochemical makeup. These variances underscore the unique metabolic roles played by each member, contributing to the collective functionality of the co-culture (Fig. 1E).

Establishing growth rates of individual consortium members from complex lignocellulosic biomass substrates

A comprehensive set of evaluations were conducted, both *in vivo* and *in silico*, to assess the performance of CTC and CTB both individually and as a consortium on complex carbon substrates, with a particular emphasis on a significant source derived from agricultural waste: deacetylated and mechanically refined corn stover (DMR). DMR is a complex composition solid resulting from applying mild alkaline and further mechanical refining treatments to corn stover solids (Chen *et al*., 2016). It primarily comprises a blend of cellulose, a homopolymer of glucose units (referred here as glucans), hemicellulose, a heteropolymer primarily composed of xylose units (referred here as xylans), and lignin, a heteropolymer composed of aromatic monomeric units. These long chain carbohydrate polymers are neither soluble nor fermentable; hence, the monomeric units must be liberated for utilization. The average composition of the DMR carbohydrate fraction consists in a ratio of 3:1 glucan to xylan. This ratio was employed to set up the initial composition of the growth media used by the models. Although other polymeric carbohydrates like galactans and arabinans are also present in DMR, their proportions are relatively small and were hence not considered in the modeling (Fig. 2A).

Experimental results confirmed that CTC externally decomposes and hydrolyzes both cellulose and hemicellulose present in DMR solids, resulting in a significant buildup of

soluble carbohydrates in the medium (Fig. 2B). This leftover supernatant, termed DMR liquor, is rich in free carbohydrate oligomers, particularly xylans and glucans, that were liberated but not consumed by CTC. Among these DMR solids decomposition by-products, CTC demonstrates a preference for assimilation of soluble cellulose-hydrolysis oligomers, specifically glucans. It has been previously described that the length of the glucan chain that CTC is able to assimilate ranges from two (cellobiose) to six (cellohexaose) glucose units (Zhang & Lynd, 2005) (Fig. 2B and 2E). Conversely, CTC exhibits an inability to assimilate pentose-based polymers derived from hemicellulose breakdown (xylans) (Fig. 2B). Notably, despite possessing a xylose transporter, CTC's consumption pathway for xylose is incomplete, lacking the enzymes xylose isomerase (XylA or Xi) and xylulokinase (XylB or Xk), both crucial for integrating this carbon source into the metabolic network through the pentose phosphate pathway. Additionally, CTC shows limited to no growth on monomeric hexoses like galactose and fructose or pentoses such as arabinose (Supplementary Table 1) (Verbeke *et al*., 2017). In contrast, CTB demonstrates consumption capabilities across various soluble carbohydrates, encompassing simple mono- and dimeric hexoses like cellobiose and glucose, as well as monomeric pentoses, i.e. xylose, both supplemented individually or as a complex mixture in the form of DMR liquor (Fig. 2C and 2E).

The benefit of utilizing a co-culture setup lies in the synergistic effect between its members. Experiments have shown that the CTC-CTB co-culture can adapt to new conditions (Fig. 2D), exemplified here by the ability to accomplish growth on insoluble complex carbohydrates and achieving increased substrate consumption compared to mono-culture setups. However, co-culture setup leads to the emergence of new metabolic interactions, which are challenging to identify by experimental setups alone. CM-models offer the advantage of easily predicting the individual growth and metabolic requirements of each member under various conditions, thereby elucidating the metabolic interactions within the community.

The CM-model *i*G^{2}1777 was used to effectively predict the growth phenotypes of CTC and CTB under both mono- and co-culture conditions (Fig. 2F). Simulation results indicated a notable reduction in growth rate for CTC in co-culture conditions, averaging approximately 90%, particularly in the presence of hexoses in the media, i.e. cellobiose, as well as in solid DMR. Additionally, CTC exhibited no growth on xylose (monomeric pentose) either individually or as part of the co-culture. Conversely, CTB showed only a slight decrease in growth rate in co-culture when consuming cellobiose and no decrease when utilizing xylose. An intriguing observation arose during simulations involving DMR as sole substrate. It was revealed that CTB did not exhibit individual growth due to its limited capacity to degrade complex carbohydrate polymers. However, as part of a co-culture, CTB experienced significant growth by leveraging the available free carbohydrates hydrolyzed by CTC. It is important to emphasize that the observed synergistic effect, enabling CTB growth in a complex lignocellulosic substrate, is accompanied by a significant decrease in the growth of CTC.

The CM-model forecasts the metabolic capabilities of the butyric acid-producing consortium

To provide valuable insights into the metabolic pathways and fermentation profiles of the consortium, both *in silico* characterization and experimental measurements of the primary fermentation by-products excreted by the two microbes (axenically and as co-culture) using DMR as a substrate were conducted (Supplementary Fig. 1). Predicted fermentation profiles were consistent with the products measured experimentally. Observations revealed that CTC undergoes mixed-acid fermentation, with formic and acetic acid (FA, AA, correspondingly) as well as ethanol (Etoh) identified as the main detected end-products, albeit in varying proportions (0.5, 4.0, and 1.2 g L^{-1} respectively) (Fig. 3A). Conversely, considerable amounts of BA (8.0 g L^{-1}) as well as AA (2.0 g L^{-1}) were measured as fermentation products for CTB (Fig. 3B). Finally, the co-culture produced a mix of all four fermentation products, though in different proportions compared to individual growth (FA 0.5 g L^{-1}, Etoh 2.6 g L^{-1}, AA 3.1 g L^{-1}, BA 2.7 g L^{-1}) (Fig. 3C). Additionally, simulations predicted that in all tested scenarios, both anaerobes excrete an extra series of common end-products, including CO_2, H_2, H^+, and H_2O (not experimentally measured) (Fig. 3D).

CM-model simulations also revealed that the consortium engages in the exchange of AA, Etoh (from CTC to CTB) (Fig. 3E), as well as a diverse array of amino acids (AAs) (Fig. F). A total of 17 AAs, including proline, serine, and valine, were exchanged, with 80% being produced in excess by CTB and transferred to CTC. Previous reports have documented excretion of AAs into the media by CTC (Yayo *et al.*, 2023), however, no studies exist indicating AAs excretion by CTB or the fate of these AAs as public goods, supporting the idea that metabolic exchanges play a crucial role in optimizing and maximizing growth and production within microbial communities. Similar examples of AAs transfer among members have been reported for other communities (Zengler *et al*., 2018; Zuñiga *et al*., 2019; Zuñiga *et al*., 2021).

By contrasting the activity across various subsystems under mono- and co-culture conditions, the metabolic functions of each member can be uncovered (Fig. 3F), unveiling a clear division of labor influenced by the distinct metabolic capacities of each participant. CTC acts as the degrader of polymers and supplier of raw materials and building blocks (xylose and AA), while CTB produces high-value compounds (BA and AAs). Nevertheless, the co-culture unveiled synergistic capabilities absent in axenic growth, enabling the microbes to surmount metabolic constraints and flourish in environments where the mono-cultures exhibit diminished performance, as demonstrated in DMR conditions with CTB suggesting a syntrophic relationship withing this community.

Exploring the interplay between acetic and butyric acid: Insights from CM-model flux dynamics

As previously noted, *i*GL^{2}1559 predicts the exchange of AA and potentially Etoh among the community members, particularly being utilized by CTB. However, experimental data and *in silico* simulations have confirmed CTB's incapability to thrive solely on AA or Etoh as a carbon source (Supplementary Table 1). The involvement of AA in CTB's BA production has been documented previously (Canganella *et al.*, 2002). A similar mechanism has also been observed in various BA-producing microbes, including bacteria found in the human gut (Louis & Flint, 2009). Simulations carried out by *i*GL^{2}1559 revealed a significant alteration in the pathway and flux distribution of the BA production system upon the introduction of AA into the medium (Fig. 4A and 4B). By quantifying the metabolic fluxes across this system, it was observed that in the absence of AA, the metabolic flux of the acetyl-CoA pool is divided between AA and BA production (22% and 63% respectively), with 100% of BA production facilitated by the Buttk enzyme (Fig. 4A). Contrary, it was forecasted that the activity across the butyryl-CoA/acetate CoA transferase (Coat) reaction contributes approximately 78% of the total flux directed towards BA synthesis when AA is introduced. This suggests that AA serves as an essential building block, facilitating the extension of the carbon chain for the synthesis of longer-chain compounds such as BA, rather than primarily being utilized for biomass generation (Fig. 4B). Previous radiolabeled carbon assays demonstrated that at least 50% of BA originates from AA (Canganella *et al.*, 2002), with up to 85% in butyrate-producing gut bacteria (Macfarlane & Macfarlane, 2003).

Additionally, through evaluations of the co-culture, it was observed experimentally and *in silico* that introducing diverse concentrations of AA into the system leads to a notable rise in BA production (Fig. 4C and 4D). Not only was there an increase in the final BA titer measured, but also in the production rate. This phenomenon has been previously documented for CTB in axenic growth (Canganella *et al*., 2002), but not as part of a consortium. On the contrary, simulations showed a metabolic trade off in which AA utilization led to a reduced growth rate (Fig. 4E). Previous studies observed a growth enhancement of 15% in CTB mono-culture upon AA supplementation (Canganella *et al*., 2002) but no studies of growth in co-culture have been reported. This implies that this process depends on additional environmental factors, triggering a switch between alternative pathways in response to media alterations. Incorporating these constraints into the computational model requires a more thorough experimental characterization and understanding of these regulatory mechanisms.

Simulations also indicated that Etoh (C2) could putatively serve as an elongation precursor for increased BA production, with the added benefit of not affecting growth (Fig. 4B and 4E). Although the CTB genome encodes a putative bifunctional alcohol dehydrogenase to convert Etoh into AA, its functional activity remains uncertain, and there is currently no conclusive experimental evidence regarding CTB's ability to uptake Etoh (Fig. 4C).

Discussion

The findings presented in this study shed light on the intricate dynamics of microbial communities and their metabolic capabilities in the context of bioconversion of renewable substrates. One of the key observations is the complementary role played by different members of the community. The presence of CTB fills the void left by CTC's inability to exploit xylans and other carbohydrates, thus allowing for single-step BA production and improved biomass conversion.

The distinctive metabolic capabilities of both CTC and CTB highlight their adaptation to mixed syntrophic growth. On one hand, CTC's ability to hydrolyze hemicellulose (rich in xylan) while showing no consumption of xylose suggests efficient access to cellulose as an energy source. Simultaneously, it facilitates the growth of other microorganisms by providing essential substrates, in exchange for other high value molecules like amino acids, which CTC can benefit from. On the other hand, evidence from both phylogenetic studies (Louis *et al*., 2007) and radioisotope analyses (Duncan *et al*., 2004) indicates the prevalence of the Coat route in butyrate-producing bacteria. This underscores the significance of AA and its ability to modulate metabolic responses in organisms from diverse ecosystems.

A significant aspect of the metabolic pathways of both CTC and CTB, akin to many other Clostridia, is the reliance on ferredoxins as electron acceptors for energy production (Guerrini *et* al., 2008). The activity within ferredoxin systems has been observed to govern energy production, fermentation profiles, and product exchange patterns. For instance, simulating an increase in the flux within ferredoxin systems results in an excessive production of reduced energy intermediates like NADH, prompting a preference for excreting less oxidized compounds such as formic acid and H_2. Conversely, limiting the flux decreases the cellular redox potential, leading to a decrease in fermentation products (such as butyrate) and an increase in the excretion of CO_2, a highly oxidized carbon molecule. These findings underscore the regulatory significance of ferredoxin-mediated redox reactions in these organisms. While the fermentation profiles predicted by the *i*GL^{2}1559 CM-model were consistent with *in vivo* measurements, our study did identify discrepancies in growth rates when compared to experimental data. These differences highlight the intricate nature of microbial community dynamics and offer valuable insights for further refining our modeling techniques to better understand and accurately represent these complex interactions.

Experimental evidence indicates that the co-culture arrangement exhibits increased substrate consumption, achieving a substantial biomass deconstruction rate of 84%, in contrast to their individual axenic cultures, this represents >100 % enhancement in substrate utilization. Despite the augmented substrate utilization and potential synergies in the co-culture there is room for further optimization, residual glucose and xylose oligomers remain at the end of the growth phase, alongside arabinan and galactan residues (Fig. 5A). It is worth noting that besides carbohydrates, significant amounts of AA (3.1 g L^{-1}) and Etoh (2.6 g L^{-1}) remain as well, with the quantity of AA comparable to the final BA titer (2.7 g L^{-1}) (Fig.s 3C and 5A).

As mentioned, these residual C2 compounds could potentially be recycled and utilized for chain elongation of BA or other valuable VFAs.

These bottlenecks suggest an opportunity for further refinement and optimization of BA production. Based on our observations, several factors were identified that could contribute to these constraints (Fig. 5B). First, there might be competition for shared resources, thus growth of one organism would hinder the growth of the other. Model simulations revealed that CTB exhibits a greater carbon uptake, suggesting a potential competitive advantage over CTC. Product inhibition may be another constraint, this VFA may primarily affect the growth and activity of CTC. Conversely, accumulation of Etoh or AA may inhibit CTB, as previously reported (Canganella *et al.*, 2002). Another potential issue restraining the system is the limitation of the overall degrading capability of the cellulosome. The enzymes in the cellulosome system may become saturated and inhibited when exposed to elevated carbohydrate concentrations, which are unlikely to be encountered in the natural environment of CTC. Additionally, it is possible that the array of enzymes present in CTC's cellulosome may not efficiently cleave the full range of carbohydrate oligomers configurations present in DMR. Further studies are required to identify the specific enzymes needed for efficient cleavage of all carbohydrate diversity of this complex substrate.

It may be possible to exploit all these residual substrates using specific pathways not found in the CTC-CTB co-culture. Although some molecular tools for these organisms exist (Mearls *et al*, 2015; Riley *et al*., 2019; Walker *et al*., 2019) they are scarce, and their development and implementation require considerable time and effort. An effective and viable approach to overcome these bottlenecks entails augmenting the current co-culture through the introduction of additional microbes that harmonize with the existing setup. These new additions should possess the requisite metabolic pathways for producing BA from the residual carbohydrates or fermentation products of the current setup. Augmentation of the co-culture can be achieved by two approaches: targeted and untargeted augmentation (Fig. 5C). The first necessitates thorough bibliographic or database exploration and leveraging CM-model guidance to pinpoint microbial strains with well-characterized attributes that align with the desired requirements. Conversely, untargeted augmentation involves the isolation and screening of microbes possessing favorable metabolic characteristics. Addressing these challenges requires a deeper understanding of the community interactions and the implementation of strategies leading to the augmentation of new members to the consortium. The utilization of co-cultures, defined consortia, and complex synthetic communities in conjunction with lignocellulosic biomass as a renewable substrate presents a promising alternative to conventional production of VFAs using petroleum-based precursors. This approach not only offers environmental benefits but also holds economic promise for the sustainable obtention of other valuable compounds.

Materials and methods

Individual GEM model construction and refinement

The corresponding genome sequences of *C. thermocellum* and *C. thermobutyricum* were downloaded from the NCBI website: https://www.ncbi.nlm.nih.gov/nuccore/CP002416 and https://www.ncbi.nlm.nih.gov/nuccore/LTAY00000000, respectively. The GEM of *C. thermocellum* (i.e. *i*CBI655, Garcia *et al.*, 2020) was obtained from: https://www.frontiersin.org/articles/10.3389/fbioe.2020.00772/full#supplementary-material. The most up-to-date and complete GEMs of *C. ljungdahlii* (i.e. *i*HN637, Nagarahan *et al*., 2013), *B. subtillis* (i.e. *i*YO844, Oh *et al*., 2007; *i*JT964-ME, Tibocha-Bonilla *et al*., 2022), and *E. coli* (i.e. *i*EC1515, Monk *et al*., 2017) were downloaded from the BIGG database (http://bigg.ucsd.edu/) (King *et al*., 2016) and provided as template models. These models were selected due to their high level of curation and extensive biological data support. An initial draft of the individual GEMs of *C. thermocellum* and *C. thermobutyricum* was generated using the RAVEN Toolbox package (Ver. 2.9.2) (Wang *et al*., 2018) for MATLAB. For the draft generation, the library uses a bidirectional homology search via BLASTp with the original genomes and the template models, assigning the best-fitting Gene-Protein-Reaction (GPR) rule. The RAVEN Toolbox function getModelFromHomology() was executed with the following cut-off parameters: a maximum E-value of 50, a minimum alignment length of 90 residues, and a minimum identity of 40%. For missing gene identifications, NCBI BLASTp was manually performed with the above parameters. To ensure quality control, drafts were subjected to iterative manual curation using the COnstraint-Based Reconstruction and Analysis (COBRApy) (Ver. 0.29) (Ebrahim *et al*., 2013), a Python software suite for quantitative analysis of biochemical networks. The remaining annotated genes were included in the model by gap filling with the help of the databases UNIPROT, BiGG (King *et al*., 2016), KEGG (Kanehisa *et al*., 2023), and MetaCyc (Caspi *et al*., 2014). Reactions were verified with experimental data when available, such as for the BA synthesis pathway (Wiegel *et al*., 1989). For reactions with no specific data available, information from the previously used template models was utilized. To aid in the gap filling and benchmarking process, relevant pathways and metabolic subsystems were visualized using the library Escher (Ver. 1.7.1) (King *et al*., 2015). To ensure standardized nomenclature and facilitate comparison between other GEMs, all reactions and metabolites in the model were named with BiGG IDs. Cellular transport systems, particularly carbohydrate uptake and amino acid transport reactions, were meticulously verified or rectified. Each metabolite in the extracellular space compartment was assigned an exchange reaction, although uptake may be restricted depending on the composition of the growth media. The biomass reaction included all essential constituents such as carbohydrates, lipids, co-factors, and vitamins, as well as their fractions in the biomass composition. For CTC, the biomass equation derived from model *i*CBI655 was used. Due to the lack of a detailed

biomass composition for CTB, the macromolecular composition of *C. ljungdahlii* represented in the model *i*HN637was used as a reference.

Community metabolic model (CM-model) generation

The generation of CM-models was carried out using COBRApy, employing a compartmentalized strategy. Initially, the individual GEMs of CTC and CTB were both placed within a unique common compartment, forming sub-partitions and a Shared Metabolite Pool (SMP). This pool allows the interconnection of individual metabolic networks and the allocation of extracellular resources, based on the uptake capabilities of each network. The SMP was populated with metabolites in line with the existing data from the individual GEMs of CTC and CTB. To distinguish common elements, prefixes corresponding to each organism were appended to each internal metabolite (i.e. glucose_CTC, glucose_CTB) and reaction (i.e. POR_CTC, POR_CTB) within the metabolic network. In the case of CTC, the suffix _CL was added to denote reactions that incorporated the cellulosome system compartment. The objective function was set to maximize biomass reactions from each individual model.

Model simulations and constrains

Individual GEM and CM-model simulations were conducted using the COBRA Toolbox with the Gurobi Optimizer (Version 5.6.3, Gurobi Optimization Inc., U.S.A) as the solver. The maximal growth rate was simulated using the Flux Balance Analysis (FBA)-associated algorithm OptCom, which aims to maximize biomass reactions. For the community, the population's growth rate was determined by the cumulative fluxes through the biomass reactions of the individual models, as shown in equation 1:

$$Model_{Objective} = Flux_{Biomass_a} + Flux_{Biomass_b} + \cdots \qquad (eq.1)$$

Simulations in different carbohydrates were executed by constraining the carbon source uptake to a maximum of 10 mmol gDW^{-1} h^{-1}. For DMR, this amount was allocated in a ratio of 7.5 mmol gDW^{-1} h^{-1} for glucose and 2.5 mmol gDW^{-1} h^{-1} xylose. No constraints were applied to the default exchange capabilities of the individual members, with all transporters being open and free to exchange. The total metabolic flux for each organism subsystem was calculated using the formula in equation 2:

$$Subsystem\_Flux_{k,j} = \sum_{i=1}^{n} Flux_{i,k,j} \qquad (eq.2)$$

The equation indicates that the total flux for a community member specific subsystem (k, j) is the sum of the individual fluxes corresponding to that subsystem. For simulations involving acetic acid and ethanol, the presence and assimilation of these compounds were achieved by

fixing the total uptake of these two molecules to 5 mmol gDW^{-1} h^{-1}. The flux was then distributed to achieve the desired proportions, maximizing the biomass growth of both community members simultaneously.

Strains, maintenance, and seed cultures preparation

Clostridium thermocellum (DSM 1313) and *Clostridium thermobutyricum* (ATCC 49875) were obtained from the Leibniz Institute DSMZ - German Collection of Microorganisms and Cell Cultures GmbH and the American Type Culture Collection (ATCC), respectively. The strains were revived under anaerobic conditions by rehydrating the pellet with 0.25 mL of culture media, then transferring the contents to a culture tube containing 5 mL of medium. From this primary culture, 2.5 mL was inoculated into each of two serum bottles containing 25 mL of culture media. These serum bottles were incubated anaerobically at 55 °C for 24-48 hours, with OD measurements taken to monitor growth. Subsequently, 0.5 mL aliquots of cultures in the exponential phase were mixed with 0.5 mL of an autoclaved mixture of 10% glycerol and 10% dimethyl sulfoxide and stored at -80 °C in sealed vials. For seed culture preparation, glycerol stocks were thawed, and 0.2 mL was transferred into a 20 mL culture medium in a serum bottle. These cultures were incubated at 55 °C at 100 rpm shaking until reaching the exponential phase and were then ready for use. Depending on the experimental setup, these seed cultures were used to inoculate a second seed in serum bottles or bioreactors.

Culture media composition and preparation

For glycerol stocks and seed cultures of *C. thermocellum* in serum bottles, CTFUD was used as the culture medium. One liter of CTFUD consisted of 3.0 g sodium citrate tribasic dihydrate, 1.3 g ammonium sulfate, 0.35 g potassium phosphate monobasic, 0.5 g L-cysteine HCl, 0.13 g calcium chloride dihydrate, 2.6 g magnesium chloride hexahydrate, 0.001 g ferrous sulfate heptahydrate, and vitamins including 0.02 g pyridoxamine dihydrochloride, 0.004 g p-aminobenzoic acid, 0.002 g D-biotin, and 0.002 g vitamin B12. Depending on the experimental campaign, CTFUD was supplemented with various carbon sources. For the fermentations conducted in this study, as well as for the glycerol stocks and seed cultures of *C. thermobutyricum* in serum bottles, the Medium for Thermophilic Clostridia (MTC) was utilized. MTC was prepared following the method described by Holwerda *et al.*, 2012, using stock solutions combined with water and the desired carbon source depending on the experimental campaign. The pH of all the media was adjusted to 7.0 using 2M KOH and then filter-sterilized. This was done using Millipore filters (Nalgene™ Rapid-Flow™ Sterile Single Use Vacuum Filter Units with PES membrane, Fisher Cat# 567-0020) or RCD (DCF 152/S; Andritz, Germany), both with a pore size of 0.2 µM. After sterilization, the media was placed in an anaerobic chamber overnight.

Seed cultures in bioreactors

C. thermocellum seed bioreactors were prepared by combining 200 mL of deionized water and 2.5 g of Avicel in each bioreactor, followed by autoclaving at 121 °C for 60 minutes. Subsequently, 250 mL of 2x MTC devoid of a carbon source and filter-sterilized were added. Once the bioreactors attained anaerobic conditions, pH 7.0, and a temperature of 55 °C, they were inoculated with 50 mL of actively growing cultures from CTFUD serum bottles. Typically, it took 10-24 hours for the seed reactors to reach the exponential growth phase, signaling readiness for transfer to the experimental bioreactors. The growth state of the cultures was monitored by observing base addition and visualizing the cultures under a microscope. *C. thermobutyricum* seed bioreactors underwent dry autoclaving at 121 °C for 60 minutes. Following autoclaving, 500 mL of filter-sterilized MTC media supplemented with 5 g L^{-1} of cellobiose and 4.5 g L^{-1} of yeast extract, was added. Upon achieving anaerobic conditions, a pH of 7.0, and a temperature of 55 °C, the bioreactors were inoculated with 50 mL of actively growing cultures from MTC serum bottles. Typically, the seed reactors required 6-8 hours to reach the exponential growth phase, signaling readiness for transfer to the experimental bioreactors. Monitoring the growth status involved measuring the OD at 600 nm and inspecting the cultures under a microscope.

Experiments in bioreactors

Bioreactor experiments in this study were maintained at a temperature of 55 ºC with stirring at 150 rpm. Nitrogen sparging at a rate of 0.1 vvm was employed to ensure anaerobic conditions. pH adjustments to 7 were made using either 2N KOH or 2N H_2SO4, with pH control during cultivations maintained using 2N KOH. Samples were aseptically collected at intervals throughout the fermentation process to assess bacterial growth, acid production, and sugar utilization. Unless specified otherwise, all fermentations were performed in duplicate. Experimental bioreactors for *C. thermocellum* were loaded with 30 g L^{-1} of DMR in 500 mL of MTC culture media. Autoclaving was carried out with the solids and 200 mL of DI water. Subsequently, 250 mL of 2x MTC devoid of a carbon source and filter-sterilized were introduced. Upon achieving the desired anaerobic conditions, pH 7.0, and a temperature of 55 °C, the bioreactors were inoculated with 50 mL of actively growing cultures sourced from seed bioreactors. *C. thermobutyricum* experimental bioreactors contained DMR liquor diluted with MTC media to a total sugar concentration of 30 g L^{-1}. The bioreactors were autoclaved dry at 121 °C for 60 minutes. After autoclaving, filtered-sterilized MTC media without sugar and supplemented with 4.5 g L^{-1} of yeast extract, and DMR liquor were added. Once the bioreactors achieved the desired anaerobic conditions, a pH of 7.0, and a temperature of 55 °C, they were inoculated with actively growing cultures from Clostridium thermobutyricum seed bioreactors to an initial OD of 0.01. Co-cultures experimental bioreactors contained 500 mL of MTC culture media with 30 g L^{-1} of DMR. The bioreactors were autoclaved with the solids and 200 mL of DI water. Then, 250 mL of 2x filter-sterilized MTC without carbon source and supplemented with 4.5 g L^{-1} of yeast extract were added. After the bioreactors achieved the desired anaerobic conditions, pH 7.0, and temperature of

55 °C, they were inoculated with 50 mL of actively growing cultures from *C. thermocellum* seed bioreactors, and with actively growing cultures from *C. thermobutyricum* seed bioreactors to an initial OD of 0.01.

Statistical methods and analysis

Data were collected from two biological replicates (n = 2) for each experimental condition. Due to the small sample size, no inferential statistical tests were performed, and error bars were not included in the figures, as the statistical power is insufficient to provide reliable estimates of variability. Instead, the mean values of the two replicates are presented, and individual data points are plotted to transparently convey the observed variability. Growth and production kinetics were predicted and characterized using the Fitderiv algorithm (Ver. 1.2) developed by Swain *et al*. (2016) with default parameters. The algorithm applies a Gaussian fit to the raw data, and the resulting fitted curves were plotted in all cases. This method effectively addresses the limitations associated with the small sample size.

Data availability

The data supporting this study are included within the paper and the supplementary information files. A reporting summary for this article is also provided as a supplementary file. Model files in were deposited within a GitHub repository: https://github.com/glastiri/Coculture. Datasets generated and analyzed during the study are available from the corresponding author upon request.

References

1. Zuñiga, C. *et al.* Environmental stimuli drive a transition from cooperation to competition in synthetic phototrophic communities. *Nat Microbiol* **4**, 2184–2191 (2019).

2. Coker, J. *et al.* A Reproducible and Tunable Synthetic Soil Microbial Community Provides New Insights into Microbial Ecology. *mSystems* **7**, e00951-22 (2022).

3. Agnihotri, S. *et al.* A Glimpse of the World of Volatile Fatty Acids Production and Application: A review. *Bioengineered* **13**, 1249–1275 (2022).

4. Linger, J. G., Ford, L. R., Ramnath, K. & Guarnieri, M. T. Development of Clostridium tyrobutyricum as a Microbial Cell Factory for the Production of Fuel and Chemical Intermediates from Lignocellulosic Feedstocks. *Front. Energy Res.* **8**, (2020).

5. Salvachúa, D. *et al.* Process intensification for the biological production of the fuel precursor butyric acid from biomass. *CR-PHYS-SC* **2**, (2021).

6. Chen, X. *et al.* A highly efficient dilute alkali deacetylation and mechanical (disc) refining process for the conversion of renewable biomass to lower cost sugars. *Biotechnology for Biofuels* **7**, 98 (2014).

7. Lamed, R., Setter, E., Kenig, R. & Bayer, E. A. Cellulosome: a discrete cell surface organelle of Clostridium thermocellum which exhibits separate antigenic, cellulose-binding and various cellulolytic activities. *Biotechnol. Bioeng. Symp.; (United States)* **13**, (1983).

8. Hirano, K. *et al.* Enzymatic diversity of the Clostridium thermocellum cellulosome is crucial for the degradation of crystalline cellulose and plant biomass. *Sci Rep* **6**, 35709 (2016).

9. Doi, R. H., Kosugi, A., Murashima, K., Tamaru, Y. & Han, S. O. Cellulosomes from Mesophilic Bacteria. *Journal of Bacteriology* **185**, 5907–5914 (2003).

10. Wiegel, J., Kuk, S.-U. & Kohring, G. W. Clostridium thermobutyricum sp. nov., a Moderate Thermophile Isolated from a Cellulolytic Culture, That Produces Butyrate as the Major Product. *International Journal of Systematic and Evolutionary Microbiology* **39**, 199–204 (1989).

11. Chi X., Li J., Wang X., Zhang J. & Antwi P. Hyper-production of butyric acid from delignified rice straw by a novel consolidated bioprocess, *Bioresource Technology* **254**, 115-120 (2018).

12. Hao, J. & Wang, H. Volatile fatty acids productions by mesophilic and thermophilic sludge fermentation: Biological responses to fermentation temperature. *Bioresource Technology* **175**, 367–373 (2015).

13. Bordbar, A., Monk, J. M., King, Z. A. & Palsson, B. O. Constraint-based models predict metabolic and associated cellular functions. *Nat Rev Genet* **15**, 107–120 (2014).

14. Kumar, M., Ji, B., Zengler, K. & Nielsen, J. Modelling approaches for studying the microbiome. *Nat Microbiol* **4**, 1253–1267 (2019).

15. Zengler, K. & Zaramela, L. S. The social network of microorganisms — how auxotrophies shape complex communities. *Nat Rev Microbiol* **16**, 383–390 (2018).

16. Zuñiga, C. *et al.* Environmental stimuli drive a transition from cooperation to competition in synthetic phototrophic communities. *Nat Microbiol* **4**, 2184–2191 (2019).

17. Zaramela, L. S. *et al.* The sum is greater than the parts: exploiting microbial communities to achieve complex functions. *Current Opinion in Biotechnology* **67**, 149–157 (2021).

18. Garcia, S. *et al.* Development of a Genome-Scale Metabolic Model of Clostridium thermocellum and Its Applications for Integration of Multi-Omics Datasets and Computational Strain Design. *Front. Bioeng. Biotechnol.* **8**, (2020).

19. Nagarajan, H. *et al.* Characterizing acetogenic metabolism using a genome-scale metabolic reconstruction of Clostridium ljungdahlii. *Microbial Cell Factories* **12**, 118 (2013).

20. Oh, Y.-K., Palsson, B. O., Park, S. M., Schilling, C. H. & Mahadevan, R. Genome-scale Reconstruction of Metabolic Network in Bacillus subtilis Based on High-throughput Phenotyping and Gene Essentiality Data *. *Journal of Biological Chemistry* **282**, 28791–28799 (2007).

21. Tibocha-Bonilla, J. D. *et al.* Predicting stress response and improved protein overproduction in Bacillus subtilis. *npj Syst Biol Appl* **8**, 1–12 (2022).

22. Monk, J. M. *et al.* iML1515, a knowledgebase that computes Escherichia coli traits. *Nat Biotechnol* **35**, 904–908 (2017).

23. Kanehisa, M., Furumichi, M., Sato, Y., Kawashima, M. & Ishiguro-Watanabe, M. KEGG for taxonomy-based analysis of pathways and genomes. *Nucleic Acids Research* **51**, D587–D592 (2023).

24. Caspi, R. *et al.* The MetaCyc database of metabolic pathways and enzymes and the BioCyc collection of pathway/genome databases. *Nucleic Acids Research* **44**, D471–D480 (2016).

25. The UniProt Consortium. UniProt: the universal protein knowledgebase in 2021. *Nucleic Acids Research* **49**, D480–D489 (2021).

26. Klitgord, N. & Segrè, D. Environments that Induce Synthetic Microbial Ecosystems. *PLOS Computational Biology* **6**, e1001002 (2010).

27. Chen, X. *et al.* DMR (deacetylation and mechanical refining) processing of corn stover achieves high monomeric sugar concentrations (230 g L−1) during enzymatic hydrolysis and high ethanol concentrations (>10% v/v) during fermentation without hydrolysate purification or concentration. *Energy Environ. Sci.* **9**, 1237–1245 (2016).

28. Zhang, Y.-H. P. & Lynd, L. R. Cellulose utilization by Clostridium thermocellum: Bioenergetics and hydrolysis product assimilation. *Proceedings of the National Academy of Sciences* **102**, 7321–7325 (2005).

29. Verbeke, T. J. *et al.* Pentose sugars inhibit metabolism and increase expression of an AgrD-type cyclic pentapeptide in Clostridium thermocellum. *Sci Rep* **7**, 43355 (2017).

30. Yayo, J. *et al.* The Roles of Nicotinamide Adenine Dinucleotide Phosphate Reoxidation and Ammonium Assimilation in the Secretion of Amino Acids as Byproducts of Clostridium thermocellum. *Applied and Environmental Microbiology* **89**, e01753-22 (2023).

31. Canganella, F., Kuk, S.-U., Morgan, H. & Wiegel, J. *Clostridium thermobutyricum*: growth studies and stimulation of butyrate formation by acetate supplementation. *Microbiological Research* **157**, 149–156 (2002).

32. Louis, P. & Flint, H. J. Diversity, metabolism and microbial ecology of butyrate-producing bacteria from the human large intestine. *FEMS Microbiology Letters* **294**, 1–8 (2009).

33. Macfarlane, S. & Macfarlane, G. T. Regulation of short-chain fatty acid production. *Proceedings of the Nutrition Society* **62**, 67–72 (2003).

34. Louis, P., McCrae, S. I., Charrier, C. & Flint, H. J. Organization of butyrate synthetic genes in human colonic bacteria: phylogenetic conservation and horizontal gene transfer. *FEMS Microbiology Letters* **269**, 240–247 (2007).

35. Duncan, S. H. *et al.* Contribution of acetate to butyrate formation by human faecal bacteria. *British Journal of Nutrition* **91**, 915–923 (2004).

36. Guerrini, O. *et al.* Characterization of Two 2[4Fe4S] Ferredoxins from Clostridium acetobutylicum. *Curr Microbiol* **56**, 261–267 (2008).

37. Mearls, E. B., Olson, D. G., Herring, C. D. & Lynd, L. R. Development of a regulatable plasmid-based gene expression system for Clostridium thermocellum. *Appl Microbiol Biotechnol* **99**, 7589–7599 (2015).

38. Riley, L. A., Ji, L., Schmitz, R. J., Westpheling, J. & Guss, A. M. Rational development of transformation in Clostridium thermocellum ATCC 27405 via complete methylome analysis and evasion of native restriction–modification systems. *Journal of Industrial Microbiology and Biotechnology* **46**, 1435–1443 (2019).

39. Walker, J. E. *et al.* Development of both type I–B and type II CRISPR/Cas genome editing systems in the cellulolytic bacterium *Clostridium thermocellum*. *Metabolic Engineering Communications* **10**, e00116 (2020).

40. King, Z. A. *et al.* BiGG Models: A platform for integrating, standardizing and sharing genome-scale models. *Nucleic Acids Research* **44**, D515–D522 (2016).

41. Kanehisa, M., Furumichi, M., Sato, Y., Kawashima, M. & Ishiguro-Watanabe, M. KEGG for taxonomy-based analysis of pathways and genomes. *Nucleic Acids Research* **51**, D587–D592 (2023).

42. Wang, H. *et al.* RAVEN 2.0: A versatile toolbox for metabolic network reconstruction and a case study on Streptomyces coelicolor. *PLOS Computational Biology* **14**, e1006541 (2018).

43. Ebrahim, A., Lerman, J. A., Palsson, B. O. & Hyduke, D. R. COBRApy: COnstraints-Based Reconstruction and Analysis for Python. *BMC Systems Biology* **7**, 74 (2013).

44. King, Z. A. *et al.* Escher: A Web Application for Building, Sharing, and Embedding Data-Rich Visualizations of Biological Pathways. *PLOS Computational Biology* **11**, e1004321 (2015).

45. Holwerda, E. K., Hirst, K. D. & Lynd, L. R. A defined growth medium with very low background carbon for culturing Clostridium thermocellum. *Journal of Industrial Microbiology and Biotechnology* **39**, 943–947 (2012).

46. Swain, P. S. *et al*. Inferring time derivatives including cell growth rates using Gaussian processes. *Nat Commun* **7**, 13766 (2016).

Acknowledgements

This material is based upon work supported by the U.S. Department of Energy, Office of Science, Office of Biological & Environmental Research under Award DE-SC0022137 and under the Secure Biosystems Design Science Focus Area (SFA) contract number DE-AC36-08GO28308. The views and opinions of the authors expressed herein do not necessarily state or reflect those of the United States Government or any agency thereof. Neither the United States Government nor any agency thereof, nor any of their employees, makes any warranty, expressed or implied, or assumes any legal liability or responsibility for the accuracy, completeness, or usefulness of any information, apparatus, product, or process disclosed, or represents that its use would not infringe privately owned rights.

Author contribution

G.L.P. and K.Z. conceived the study. M.K. helped construct the initial models' drafts. G.L.P. developed individual GEM models, the CM-model and computational methods as well as performed simulations and experimental designs. L.M., N.H., V.S.N. performed bioreactor experiments and substrate and byproducts measurement with input from J.L and M.G. Results were discussed by G.L.P, L.M., M.G. and K.Z. G.L.P. and L.M. analyzed the data. G.L.P. wrote the manuscript with input from all co-authors.

Competing interests

The authors declare no competing interests.

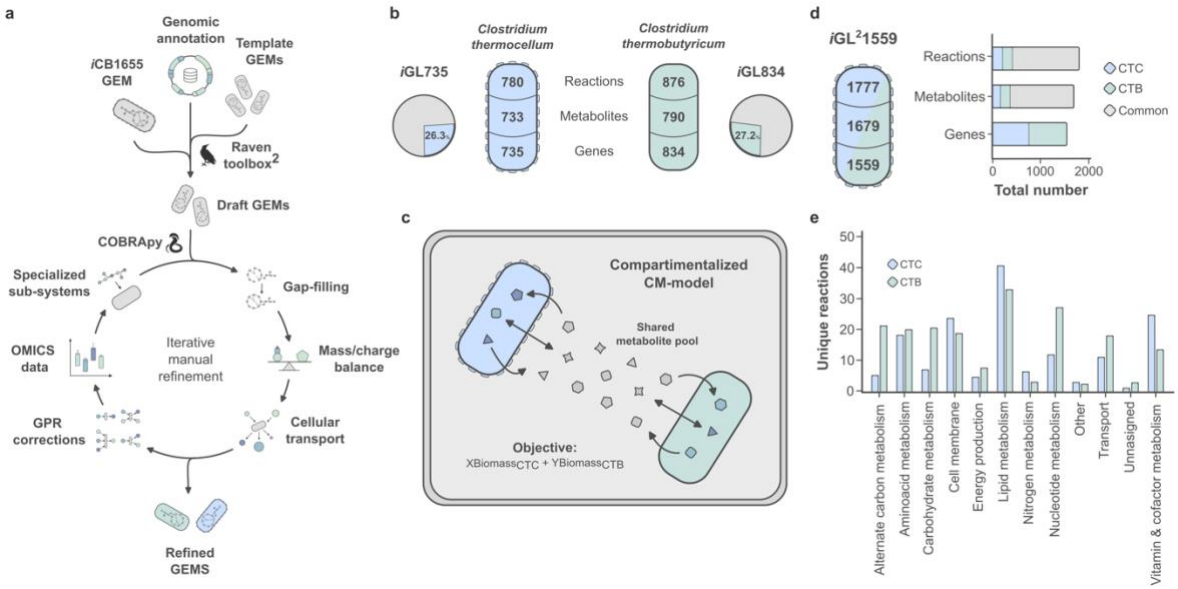

Fig. 1: Construction of individual and community metabolic models: process and features. a Initial draft models of *Clostridium thermocellum* (CTC) and *Clostridium thermobutyricum* (CTB) were constructed using different information sources and the RAVEN Toolbox (Wang *et al*., 2018), followed by iteratively manual curation using COBRApy (Ebrahim *et al*., 2013), and biological information. **b** Key attributes of the final curated individual genome scale metabolic models (GEMs), with the pie chart indicating the percentage of genomic coverage. **c** Depiction of the structure of the two individual GEMs merged into a compartmentalized community metabolic model (CM-model), featuring a shared metabolite pool (SMP) and a composite objective considering growth for both members. **d** Overall properties of the *i*GL^{2}1559 CM-model, colors in the bars represent exclusive features coming from each individual GEM, while gray denotes common or shared features. **e** Distribution of unique reactions across different metabolic subsystems of each individual.

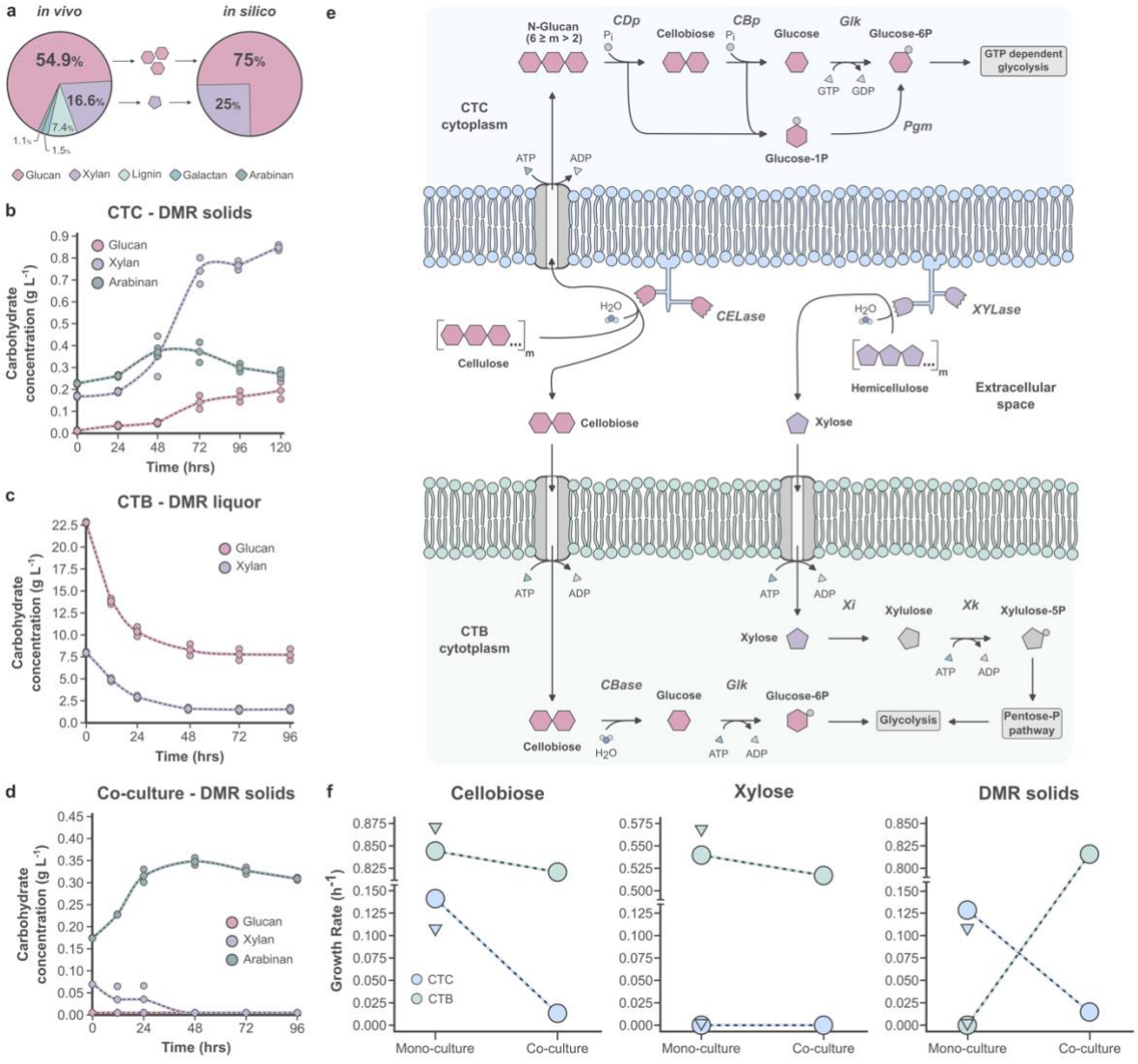

Fig. 2: Co-culture carbohydrate substrate uptake capabilities. a Deacetylated and mechanically refined corn stover (DMR) average composition used in *in vivo* growth setups (left). Carbohydrate ratio used to perform growth simulations with DMR as carbon substrate (right). **b** Profile of experimentally measured *Clostridium thermocellum* (CTC) free soluble carbohydrate excretion after growth on DMR solids. **c** Profile of experimentally determined *Clostridium thermobutyricum* (CTB) free soluble carbohydrate consumption derived from growth on DMR liquor. **d** Profile of experimentally measured free soluble carbohydrate excretion/consumption for the CTC-CTB consortium using DMR solids as substrate. In all cases, circle markers indicate individual measurements obtained from independent samples (n = 2), while diamonds represent the mean. The line represents the predicted production kinetics using a Gaussian fit (see Methods). Please note the different y-axis scales in panels b-d. **e** *Top:* Representation of modeled carbohydrate hydrolysis and metabolism in CTC. Cellulose and hemicellulose are subjected to enzymatic degradation in the cellulosome by cellulases (CELase) and xylanases (XYLase). Hydrolyzed glucans (glucose monomers (Glu_m) ≤ 6) are transported into the cell via ABC-type transporters. Upon internalization, glucans undergo phosphorolytic cleavage by cellodextrin phosphorylase (CDPase) to yield glucose-

1-phosphate (G1P) and a glucan molecule shortened by one glucose unit, iteratively reducing its length until cellobiose (Glu_m = 2) is obtained. Cellobiose is subsequently cleaved by cellobiose phosphorylase (CBPase) to produce glucose and G1P. Glucose is further converted by glucokinase (Glk) to glucose-6-phosphate (G6P). G1P molecules are converted to G6P by phosphoglucomutase (Pgm), which are then channeled into a GTP driven glycolytic pathway. *Bottom*: Visualization of the modeled carbohydrate uptake and metabolism in CTB. Hydrolyzed glucans ($Glu_m \leq 2$) are transported into the cell via ABC-type transporters. Once inside, cellobiose is split into two glucose units by cellobiose hydrolase (CBHase). Glucose then gets converted to G6P by Glk and fed into the glycolytic pathway. Additionally, hydrolyzed xylose is internalized via ABC-type transporters and then converted into xylulose by xylose isomerase (Xi) and subsequently phosphorylated by xylulokinase (Xk) to yield xylulose-5-phosphate, which follows the pentose phosphate pathway producing intermediates for glycolysis. **f** Growth rates for CTC and CTB, both individually and in co-culture across the various carbohydrates present in DMR. Circles represent the *in silico* predicted rates, assuming a total carbon source uptake of 10 mmol gDW^{-1} h^{-1}, while triangles indicate experimentally determined growth rates based on measurements from independent samples (n = 2), inferred using time derivatives (see Methods).

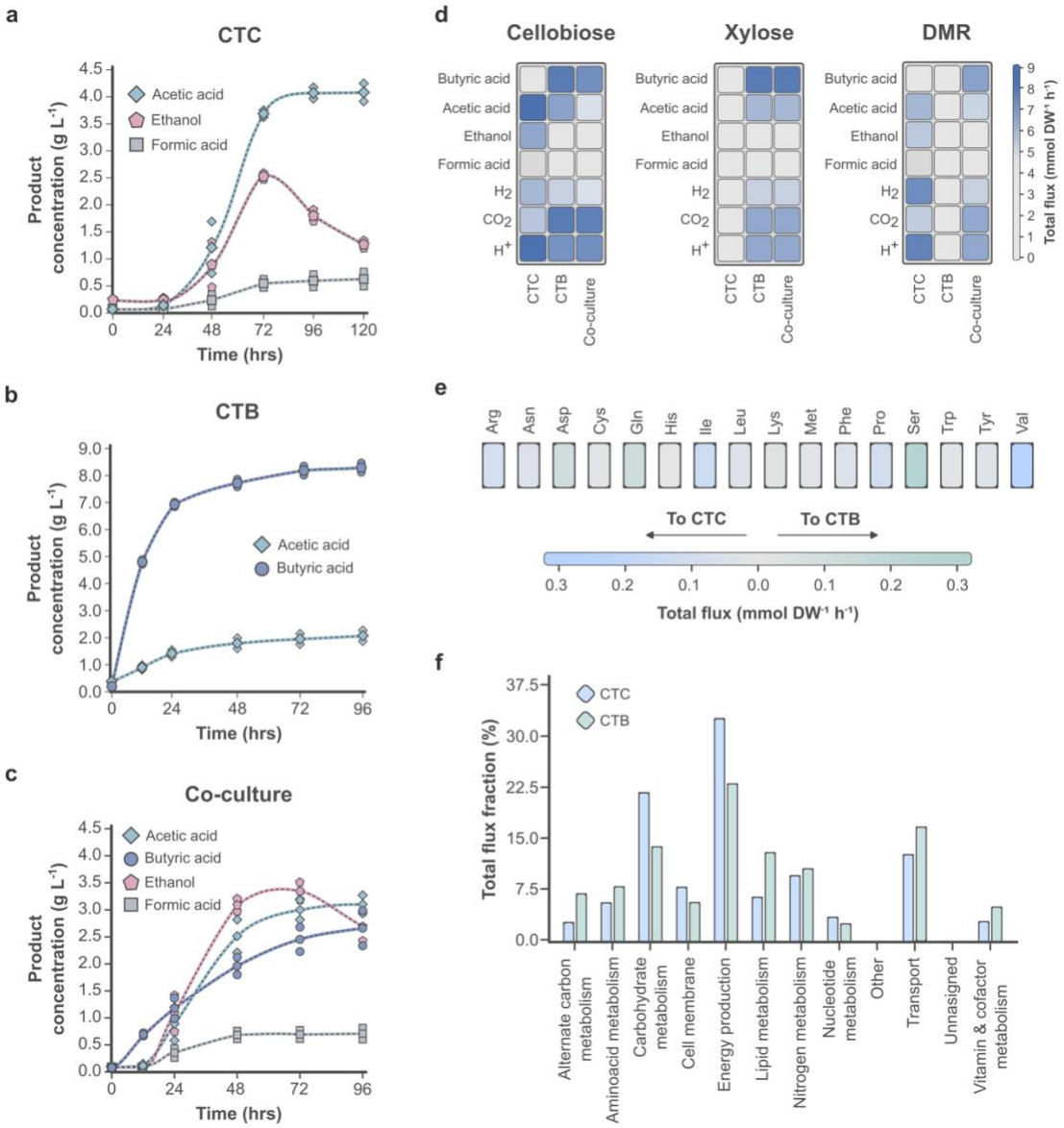

Fig. 3: Fermentation profiles of the Syn-com. a *In vivo* fermentation profile of *Clostridium thermocellum* (CTC) cultivated on mechanically refined corn stover (DMR). **b** Fermentation profile of *Clostridium thermobutyricum* (CTB) during growth on DMR liquor. **c** Fermentation profile of CTC-CTB co-culture grown on DMR. In all cases, circle markers indicate individual measurements obtained from independent samples (n = 2). The line represents the predicted production kinetics using a Gaussian fit (see Methods). Note the different y-axis in panels b-d. **d** Predicted fermentation profiles of the community and its constituent members using *in silico* simulations for hexoses (cellobiose), pentoses (xylose) and DMR (cellobiose and xylose). Color intensity reflects the quantity of excreted products (mmol DW^{-1} h^{-1}). **f** Heatmap depicting the amino acid (AAs) exchange among members. Green indicates AAs produced in excess by CTC and consumed by CTB, while blue indicates AAs produced by CTB and consumed by CTC. Intensity of color denotes the amount exchanged (mmol DW^{-1} h^{-1}). **g** Allocation of metabolic flux quantities across various subsystems within the individual community members.

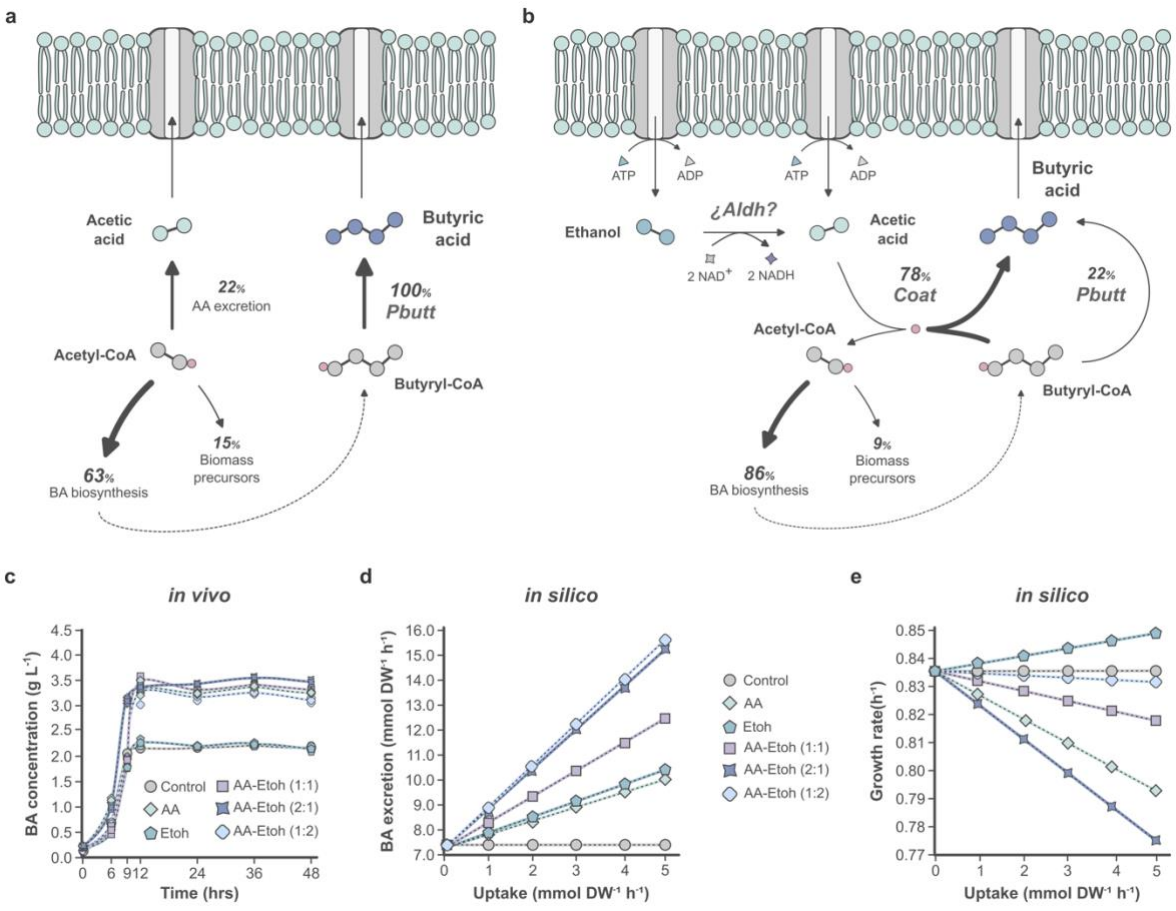

Fig. 4: Dynamics of acetic acid (AA) and butyric acid (BA) production systems. a Flux dynamics in BA production without AA addition. **b** Fluxomic analysis of BA biosynthesis pathways with AA (and putatively ethanol, Etoh) supplementation in the medium. **c** *In vivo* butyrate production of the co-culture across distinct proportions of AA to Etoh addition. In all cases, markers indicate individual measurements obtained from independent samples (n = 2) and the line represents the predicted production kinetics using a Gaussian fit (see Methods). **d** *In silico* assessment of BA production by the co-culture with varied concentrations and ratios of AA to Etoh. **e** Growth rate predictions of the co-culture across varied concentrations and ratios of AA to Etoh.

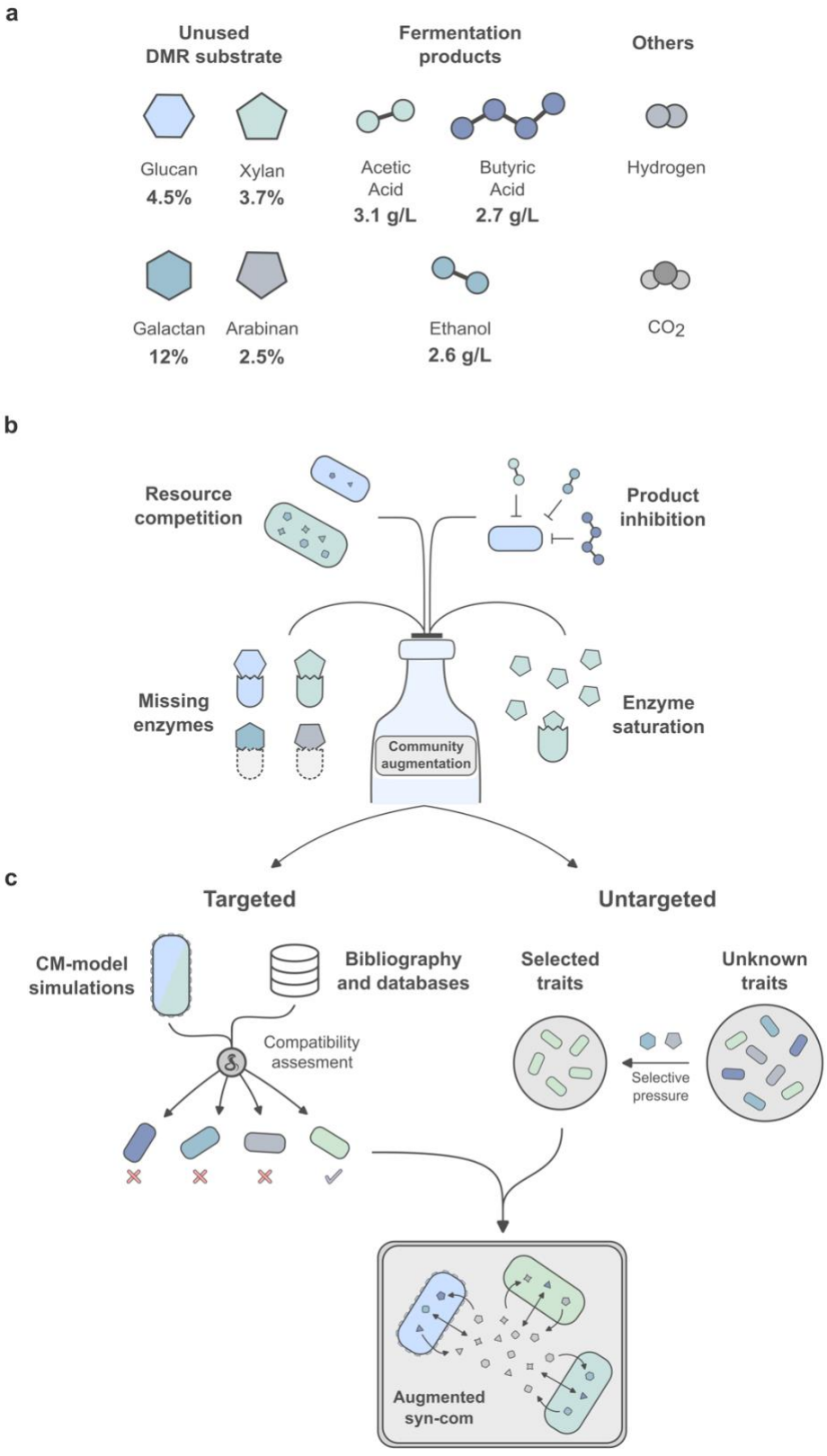

721

722 **Fig. 5: Butyric acid (BA) production bottlenecks and potential framework for optimization. a**
723 Residual substrates and fermentation by-products of the co-culture cultivated in deacetylated and

mechanically refined corn stover (DMR). **b** Primary factors contributing to bottlenecks in BA production. **c** Enhancing strategies proposed for co-culture augmentation.

Model ID	*i*CBI665	*i*HN637	*i*YO844	*i*ML1515	*i*GL735	*i*GL834
Genes	665	637	844	1515	735	834
Reactions	795	785	1250	1877	780	876
Metabolites	854	698	990	2712	733	790
Genome Coverage	24%	15%	20%	33%	26%	27%
Microorganism	*Clostridium thermocellum*	*Clostridium ljungdahlii*	*Bacillus subtillis*	*Escherichia coli*	*Clostridium thermocellum*	*Clostridium thermobutyrycum*
Reference	Garcia *et al*., 2020	Nagarahan *et al*., 2013	Oh *et al*., 2007	Monk *et al*., 2017	This study	This study

726

727 **Table 1. Overview of the main features of the GEM models utilized and developed in this study.**